ELSEVIER

Contents lists available at ScienceDirect

Journal of Colloid and Interface Science

journal homepage: www.elsevier.com/locate/jcis



Evaluating the Rheo-electric Performance of Aqueous Suspensions of Oxidized Carbon Black



Paolo Zapanta Ramos^a, Connor Clayton Call^{a,1}, Lauren Virginia Simitz^{a,2}, Jeffrey John Richards^{a,*}

^a Department of Chemical and Biological Engineering, Northwestern University, Evanston, IL 60208, USA

HIGHLIGHTS

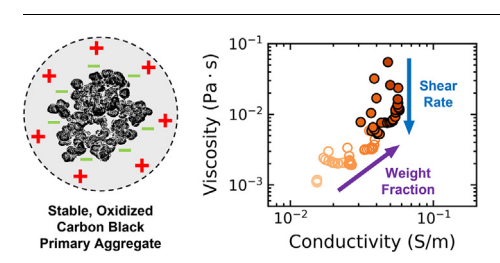
- Repulsive interaction of oxidized carbon black reduced agglomeration.
- Onset of solidification was shifted to higher particle loadings.
- Electronic conductivities of aqueous suspensions were independent of shear intensity.
- Lower viscosity, higher conductivity fluid suspensions were formed.
- Electrostatic stability does not lead to desired conductive additive performance.

ARTICLE INFO

Article history:
Received 19 September 2022
Revised 30 November 2022
Accepted 5 December 2022
Available online 11 December 2022

Keywords:
Carbon black
Conductive additive
Flow electrode
Surface oxidation
Rheo-electric characterization
Colloidal stability

G R A P H I C A L A B S T R A C T



ABSTRACT

Hypothesis: The macroscopic properties of carbon black suspensions are primarily determined by the agglomerate microstructure built of primary aggregates. Conferring colloidal stability in aqueous carbon black suspensions should thus have a drastic impact on their viscosity and conductivity.

Experiments: Carbon black was treated with strong acids following a wet oxidation procedure. An analysis of the resulting particle surface chemistry and electrophoretic mobility was performed in evaluating colloidal stability. Changes in suspension microstructure due to oxidation were observed using small-angle X-ray scattering. Utilizing rheo-electric measurements, the evolution of the viscosity and conductivity of the carbon black suspensions as a function of shear rate and carbon content was thoroughly studied.

Findings: The carboxyl groups installed on the carbon black surface through oxidation increased the surface charge density and enhanced repulsive interactions. Electrostatic stability inhibited the formation of the large-scale agglomerates in favor of the stable primary aggregates in suspension. While shear thinning, suspension conductivities were found to be weakly dependent on the shear intensity regardless of the carbon content. Most importantly, aqueous carbon black suspensions formulated from electrostatically repulsive primary aggregates displayed a smaller rise in conductivity with carbon content compared to those formulated from attractive agglomerates.

© 2022 Elsevier Inc. All rights reserved.

Abbreviations: CB, carbon black; C–OH, hydroxyl group; C=O, carbonyl group; COOH, carboxyl group; DI, deionized; DLS, dynamic light scattering; FCDI, flow-electrode capacitive deionization; HCl, hydrochloric acid; HNO3, nitric acid; H2SO4, sulfuric acid; NaCl, sodium chloride; NaOH, sodium hydroxide; TEM, transmission electron microscopy; USAXS, ultra-small-angle X-ray scattering; XPS, X-ray photoelectron spectroscopy.

^{*} Corresponding author.

E-mail addresses: paoloramos2024@u.northwestern.edu (P.Z. Ramos), cccall@stanford.edu (C.C. Call), lvsimitz@stanford.edu (L.V. Simitz), jeffrey.richards@northwestern.edu (J.J. Richards).

¹ Present address: Department of Chemical Engineering, Stanford University, Stanford, California, 94305, USA.

² Department of Aeronautics and Astronautics, Stanford University, Stanford, California, 94305, USA

1. Introduction

Seawater and brackish water are promising sources for obtaining potable water beyond what the hydrological cycle provides. An emerging water desalination technology that promises to deliver high salt removal efficiency with scalable, continuous operation is flow-electrode capacitive deionization (FCDI) [1]. FCDI replaces the static, porous electrodes in conventional capacitive deionization systems with conductive suspensions know as flow electrodes. Flow electrodes used for FCDI consist of activated carbon with a conductive additive dispersed in an aqueous solution [2,3]. The activated carbon provides a large, pseudo-capacitance, originating from its high specific surface area that traps ions in its electrical double layer under an applied electric field [4,5]. In contrast, the conductive additive, usually a nanoscale carbonaceous species, facilitates electrical transport through the suspension by enhancing charge transport from the current collectors to the activated carbon particles as they are convected down the flow channel [3]. Unfortunately, the addition of the conductive additive causes detrimental effects to the viscosity of the flow electrode. At particle loadings necessary to achieve high electrical conductivities, it is often observed that the viscosity of flow electrodes can exceed 10 Pa·s [6]. This leads to unacceptable pumping costs that affect system level performance [7,8]. A balance between high conductivity and low viscosity must be achieved for any suspension electrode to ensure mitigation of ohmic losses electrochemical cycling.

To this end, high-structured carbon black particles are commonly used as conductive additives in electrochemical energy storage devices and electrically conducting nanocomposites as they allow for a higher electrical conductivity with fewer mass of added carbon [9-12]. The rheological properties of carbon black arise from its complex microstructure hierarchy. At the nanoscale level are porous primary particles that are chemically fused to create fractal primary aggregates that are typically 100 nm in diameter [13,14]. The primary aggregates make up the colloidal building blocks in these suspensions, interacting to produce reversible fractal agglomerates. Agglomeration in aqueous suspensions is often explained using the Derjaguin, Landau, Verwey, and Overbeek theory, stating that forces acting between two particles in suspension are a balance of electrostatic repulsion and Van Der Waal's attraction [15,16]. In order to control this balance, several research groups have functionalized the surface of activated carbon [17,18] and carbon nanotubes [19,20], another conductive additive, in an effort to minimize agglomeration by enhancing electrostatic stability. While successful, open questions remain regarding how surface functionalization affects the colloidal interactions that dictate both the rheology and conductivity of these suspensions. The lack of understanding leaves no clear direction towards engineering flow electrodes with improved performance.

In our work, we provide a quantitative comparison of the rheoelectric behavior of carbon black particles suspended in water. We compare dense suspensions formulated from oxidized Vulcan XC72R carbon black (CB) to that of the pristine material. We show that oxidation results in an enhanced surface charge density and electrostatic stability due to the installation of carboxyl groups. Using ultra-small-angle X-ray scattering, we quantify the microscopic effects of oxidation and show that the electrostatic stabilization is maintained with increasing carbon loadings. As a result, oxidation leads to a shift in the onset of the fluid-solid transition to higher weight fractions. Finally, we evaluate the rheo-electric behavior of dense suspensions of both pristine and oxidized CB in flow and compare the evolution of the viscosity to the electrical conductivity as a function of shear rate and particle loading. While oxidation of the CB particles leads to reduced suspension viscosities, we find a trade off in the electrical performance. Oxidized

CB displays higher conductivities when the suspensions are a fluid, but pristine CB exhibits a greater rise in conductivity with increasing particle loadings past solidification.

2. Materials and methods

2.1. Materials

Vulcan XC72R carbon black (CB) was purchased from Cabot Corporation (Boston, MA, USA). 98 wt% sulfuric acid (H_2SO_4), 70 wt% nitric acid (HNO_3), and 38 wt% hydrochloric acid (HCI) were obtained from Thermo Fisher Scientific (Waltham, MA, USA). Sodium bicarbonate, sodium hydroxide (NaOH), and sodium chloride (NaCl) were bought from MiliporeSigma (St. Louis, MO, USA). 10 kDa dialysis tubing was obtained from Spectrum Chemical (New Brunswick, NJ, USA). 0.15 μ S/cm deionized (DI) water was used for all experiments.

2.2. Oxidation procedure

Acid oxidation of the CB surface follows a similar procedure previously performed on carbon nanotubes [21]. CB was refluxed in a concentrated acid mixture of 3:1 vol/vol $\rm H_2SO_4$ and $\rm HNO_3$ at 80 °C for 4 hr, and then washed with DI water by centrifugation (4000 rpm) for 10 min repeatedly until the supernatant exhibited a pH above 4. The collective precipitate was resuspended in DI water and neutralized to a pH of 7 with sodium bicarbonate. Excess salts were extracted via dialysis until the conductivity of the DI water dialysate buffer was maintained below 5 $\mu S/cm$ overnight. The oxidized sample was freeze dried at -55 °C under vacuum for a minimum of 3 days.

2.3. Suspension preparation

CB was dispersed in neat DI water using two methods depend-CB the content (w) defined ing on $w = \frac{\text{Dry Carbon Black Weight}}{\text{Total Suspension Weight}} \times 100\%$. Any conversions to volume fraction were performed using an assumed dry CB density of 1.8 g/ mL. Dilute CB suspensions (w < 1 wt%) were bath sonicated for 30 min to break down the agglomerates to its primary aggregate building block. Concentrated CB suspensions ($w \ge 1$ wt%) were prepared using a five-step method, consisting first of vortex mixing at 3000 rpm for 2 min that then alternates with bath sonication for at least 10 min. The latter preparation method was necessary to thoroughly disperse CB in water and break down the attractive agglomerates, leading to a reversible, thixotropic suspension [22]. These preparation procedures were repeated prior to any measurements of the CB suspensions to prevent the effects of sedimentation or colloidal phase separation.

2.4. Characterization

High-resolution images of the particles were taken with a JEOL 2100F transmission electron microscope (TEM) with a Schottky field emission gun operated at 200 kV. X-ray photoelectron spectroscopy (XPS) was performed using a Thermo Scientific ESCALAB 250Xi with a 500 μm monochromatic Al K α X-ray source. Emitted binding energies were charge-shifted to reference adventitious carbon at 284.8 eV. Peak fitting analysis was performed using the Thermo Fisher Scientific Avantage Datasystem software. The zeta potential as a function of pH was measured using a Malvern Instruments Zetasizer Nano ZS with DTS1070 capillary cells. A 5 mM NaCl stock solution was prepared and shifted to a pH of 4 and 10 with the addition of HCl and NaOH, respectively. With the same zeta instrument and holder, the hydrodynamic size of the primary

aggregates was calculated through dynamic light scattering (DLS) with a 173° detection angle (backscattering). Measurements were taken every 30 sec for approximately 30 min with dispersants of increasing NaCl concentration. The CB microstructure was evaluated with ultra-small-angle X-ray scattering (USAXS) on the Advanced Photon Source 9ID beamline at Argonne National Labs [23,24]. Scattering intensities were collected in a wavevector range of 1×10^0 to 1×10^{-4} Å $^{-1}$. The data was corrected for slit smearing and the scattering contribution of the solvent using IGOR Pro reduction macros [25].

2.5. Rheo-electric measurements

Rheological measurements were completed using a TA Instruments ARES-G2 strain-controlled rheometer with a custom-built Couette geometry (titanium, inner diameter = 26 mm, outer diameter = 27 mm) that simultaneously allows for dielectric spectroscopy measurements using a Keysight E4990A Impedance Analyzer (FigS1) [26]. The planar gap at the base of the geometry was set to 0.5 mm. All measurements were maintained at 25 °C using a forced convection oven. Mechanical percolation of the CB microstructure was characterized through small amplitude oscillatory shearing. A 0.5% strain amplitude was applied to the samples ranging from 10 to 0.1 rad/s. Flow curves were constructed using a previously established protocol that eliminates the effects of aging and sedimentation in CB suspensions [13,27]. A constant shear rate was applied to the suspensions starting from 2500 s⁻¹ to 10 s⁻¹ for 5 min at each shear rate of interest, separated by a preshear step at 2500 s⁻¹ for 5 min to erase structural history. A necessary correction of the measured shear stresses was administered for the contribution of the geometry solvent trap (FigS2). The complex impedance of the CB suspensions was taken in the direction of the shear gradient, perpendicular to the cup and bob walls, over a frequency (f) range of 20 Hz to 5 MHz. The measured response was corrected for the residual impedance of the wires and stray admittance of the open circuit using standard corrections [26]. The sample conductivity (κ) was calculated from the corrected complex impedance (Z^*) using the equation $\kappa = Re(C/Z^*)$ where Cis the cell constant calibrated using salt solutions of known conductivity and Re signifies the real component of the complex number.

3. Results and discussion

3.1. Surface chemistry and charge

Acid oxidation of the CB surface was accomplished by refluxing dry particles in a concentrated acid mixture of 3:1 vol/vol H₂SO₄ and HNO₃ at 80 °C for 4 hr. After washing and neutralization, oxidation was confirmed using an XPS survey scan of the dry pristine and oxidized CB powder (Fig. 1a). The scan was truncated to highlight the carbon (C 1s) and oxygen (O 1s) peaks. Oxidized CB exhibits an increase in the O 1s peak relative to the C 1s peak from 0.02 to 0.08, indicating the installation of oxygen-containing functional groups. A small trace of sulfur was detected comprising less than \sim 0.4 and \sim 0.2 atomic % for pristine and oxidized CB, respectively. This sulfur impurity is normally found on the surface of commercial XC72R [28,29] and can be selectively removed following acid treatment [29]. The notable absence of nitrogen and residual sulfur content confirms effective removal of excess acids during the washing procedure. The high-resolution C 1s spectra were analyzed to track the detailed change in the surface chemistry due to oxidation (Fig. 1b). The C 1s spectra were fit to 6 peaks: 1 graphite peak (C—C, 284.40 eV); 3 oxygen functional group peaks of hydroxyls (C-OH, 285.90 eV), carbonyls (C=O, 287.4 eV), and carboxyls (COOH, 289.00 eV); and 2 satellite peaks ($\pi \to \pi^*$, 290.90 and 293.40 eV) [28]. The center positions were restricted to fall within 0.2 eV of referenced literature values. The full width at half maximum was allowed to float but matches for each peak between the two samples. The resulting areas of the assigned peaks are summarized in Table 1. The C—C graphite peak dominates the C 1s spectra for both samples. After oxidation, the oxygen-containing functional group peak intensities increase relative to the graphite peak, consistent with the increase in oxygen content observed in XPS survey scan. Interestingly, oxidized CB also exhibits a larger $\pi \to \pi^*$ peak intensity. These $\pi \to \pi^*$ satellite peaks are normally associated with the polycyclic aromaticity of the carbon sample and thus its capability for intraparticle electron transport [30]. The oxidized CB remains conductive and its intrinsic electrical transport properties far exceed that of the suspensions tested here.

The installation of additional oxygen functional groups on the CB surface inherently modifies its surface charge. The zeta potential of 0.01 wt% CB suspensions at a pH of 3, 7, and 10 was measured to quantify changes in surface charge due to the modified surface chemistry (Fig. 1c). Pristine CB exhibits a zeta potential of 26.1 ± 1.6 mV at a neutral pH, too weak to overcome Van der Waal's forces. As the pH increases from acidic conditions, the magnitude of the zeta potential decreases until charge inversion occurs. Overcharging of particles suspended in a polar protic solvent, such as water, can be attributed to ion correlation effects [31,32]. While the exact origin of this phenomenon remains uncertain, in part from the batch reliant chemical nature of Vulcan XC72R, its zeta potential is strongly pH dependent. In contrast, oxidized CB exhibits a larger zeta potential of -56.6 ± 3.1 mV at a neutral pH that remains negative across the range of pH measured. The larger, negative surface charge combined with the enhanced oxygen functionality of the XPS measurements are consistent with the presence of installed carboxyl groups (COOH) on the CB surface that dissociate to carboxylate anions (COO⁻) in water at pH > 3 [16,33]. The degree of dissociation lessens in acidic conditions as evident from the decrease in magnitude of the zeta potential, consistent with what is observed in other oxidized carbonaceous species such as carbon nanotubes [19.33]. The pH dependence of the zeta potential for pristine CB reveals the origin of its poor colloidal stability in water. Installation of carboxyl groups upon oxidation and the resulting increase in surface charge is therefore key in formulating stable suspensions in DI water.

3.2. Colloidal interactions

The enhanced stability of oxidized CB suspensions was quantitatively examined using the stability ratio, defined as the ratio of the rapid and slow agglomeration rates of the primary aggregates. The hydrodynamic size of the CB colloids was measured using DLS over a 30 min time scale after rigorous bath sonication. The measured characteristic time scale of agglomeration (τ_{agg}) is directly related to the stability ratio (W) following $\tau_{agg} = \pi \eta_m a^3 W / \phi k_B T$ [34]. Here, is the viscosity of water, *a* is the hydrodynamic radius, ϕ is the CB volume fraction, is Boltzmann's constant, and T is the absolute temperature. Stability ratios were plotted as a function of NaCl concentration for pristine and oxidized suspensions (Fig. 2a). At 5 mM, the lowest NaCl concentration measured, pristine CB already holds a low stability ratio of \sim 1 indicating poor stability [34]. This results in the formation of large agglomerates that sediment to the bottom of the container (Fig. 2b). At the equivalent NaCl concentration, oxidized CB shows enhanced stability with a stability ratio over 10 and increased dispersibility in water. TEM images along with additional DLS measurements confirmed that the oxidation procedure had no effect on altering the size of the primary particle or breaking down the primary aggregates (FigS3

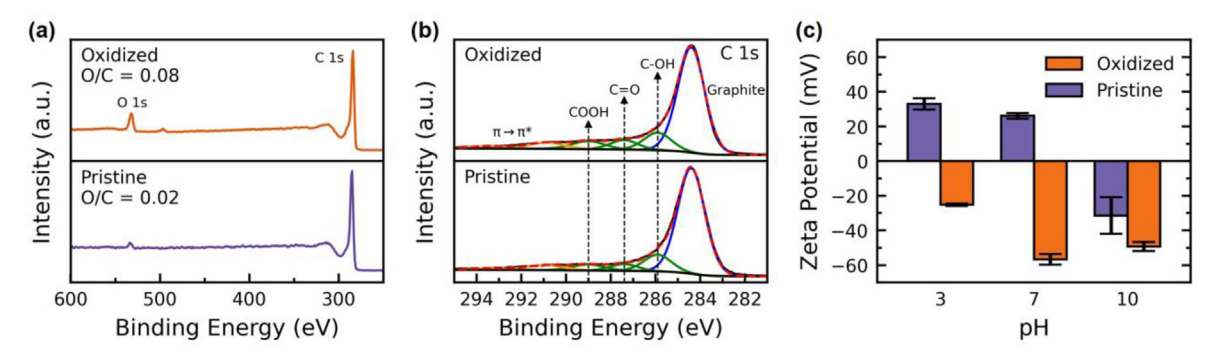


Fig. 1. (a) XPS survey scan of the CB particles. Oxygen to carbon ratios (O/C) are calculated from the atomic percentage of each element (b) High-resolution XPS analysis of the carbon spectra. Arrows denote peak position of carbon-oxygen functional groups. (c) Zeta potential measurements as a function of pH calculated from the electrophoretic mobility of the CB particles. Error bars are 1 standard deviation from the average of 3 measurements.

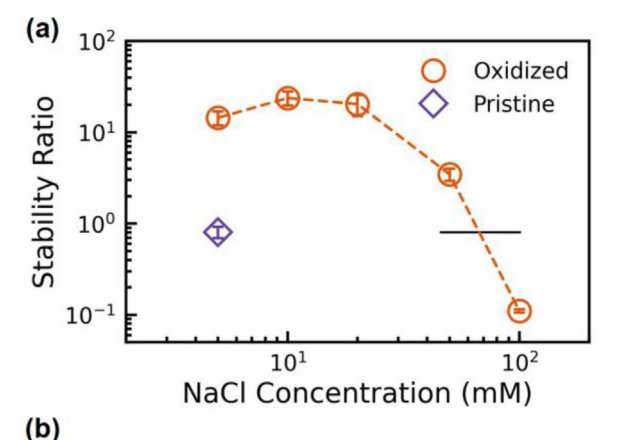
Table 1Relative peak areas (%) of the fitted C 1s peaks from the carbon XPS spectra.

Sample	C—C	C-OH	C=0	СООН	$\pi \to \pi^*\left(I\right)$	$\pi \to \pi^* (II)$
Pristine XC72R	73.15	10.93	4.66	4.92	4.70	1.64
Oxidized XC72R	66.99	12.46	6.41	6.33		2.29

and S4). The stark difference in the stability of the two CB samples thus signifies reduced agglomeration of the primary aggregates by enhanced electrostatic stability of the oxidized CB. The electrostatic nature of the stability is confirmed by the trend of the stability ratio for oxidized CB with NaCl concentration. At high ionic strengths above 20 mM, a dramatic decline in stability is observed. This indicates that the suspension is at its critical coagulation concentration, with higher salt concentration leading to enhanced agglomeration [34]. This behavior is similar to that observed by Gloukhovski et al. who reported enhanced agglomeration of multi-walled carbon nanotubes in suspension with the addition of potassium bromide [35]. Above 100 mM, the improved stability compared with the pristine suspension is lost, as the surface charge conferred from the deposited carboxylate anions are fully shielded by the salts in the solution [31].

The change in the nanoscale interactions from net attraction to repulsion is also reflected in the CB microstructure, confirmed using USAXS. The background subtracted scattering intensity (I) vs. wavevector (Q) for pristine and oxidized CB at 2.7 wt% is shown in Fig. 3a. At high-Q ($\dot{Q} > 2 \times 10^{-2} \text{ Å}^{-1}$), the scattering intensity is dominated by the form factor of the primary particles. The similarity in the scattering features between the pristine and oxidized samples in this region confirms that the oxidation procedure did not significantly alter the internal structure of the primary particles. At low-Q (Q < $4 \times 10^{-3} \text{ Å}^{-1}$), however, the effects of oxidation on the microstructure become apparent. The pristine sample shows a strong increase in scattering intensity with decreasing Q. exhibiting a power-law slope ($I \sim Q^n$) of n = -3.9 that is consistent with the formation of CB agglomerates exceeding many micrometers in diameter [27]. In contrast, the low-Q scattering from the oxidized sample nears a plateau, confirming the enhanced electrostatic stability conferred by oxidation.

To investigate the influence of particle loading on the microstructure and confirm the trend at low Q-values, the CB content was diluted from 2.8 to 0.2 wt%. The background subtracted scattering intensity at each CB content was normalized to the intensity in the form-factor region, Q-values between 1×10^{-2} and 1×10^{-1} Å $^{-1}$, and the resulting profiles are shown in Fig. 3b. and 3c. for pristine and oxidized CB respectively. For pristine CB, there is no apparent concentration dependence of normalized scattering intensity at the probed length scales as the CB content



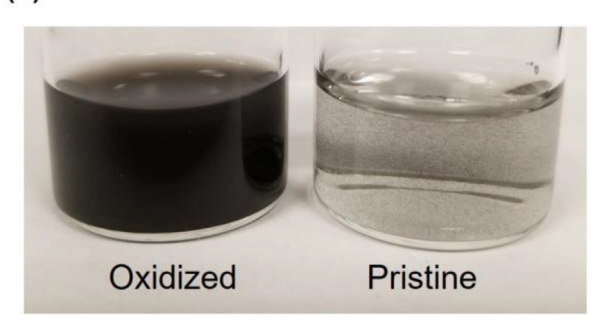


Fig. 2. (a) Stability ratios of pristine and oxidized CB suspensions at 0.01 wt% as a function of NaCl concentration. Error bars are 1 standard deviation calculated from the variance of the estimated stability ratio from the curve fit of 1 measurement. The dashed lines between subsequent points are meant to guide the eyes. The horizontal solid line denotes stability ratio of pristine CB in 5 mM NaCl. (b) Optical images of 0.01 wt% CB suspensions in 5 mM NaCl taken 30 min after bath sonication.

increases. This is consistent with prior studies of CB suspensions in propylene carbonate, which was attributed to the formation of micron-sized CB clusters of definite size prior to mechanical percolation [23]. On the other hand, the scattering intensity decreases with increasing CB content for oxidized CB. This is a direct manifestation of the enhanced electrostatic stability that is made possible

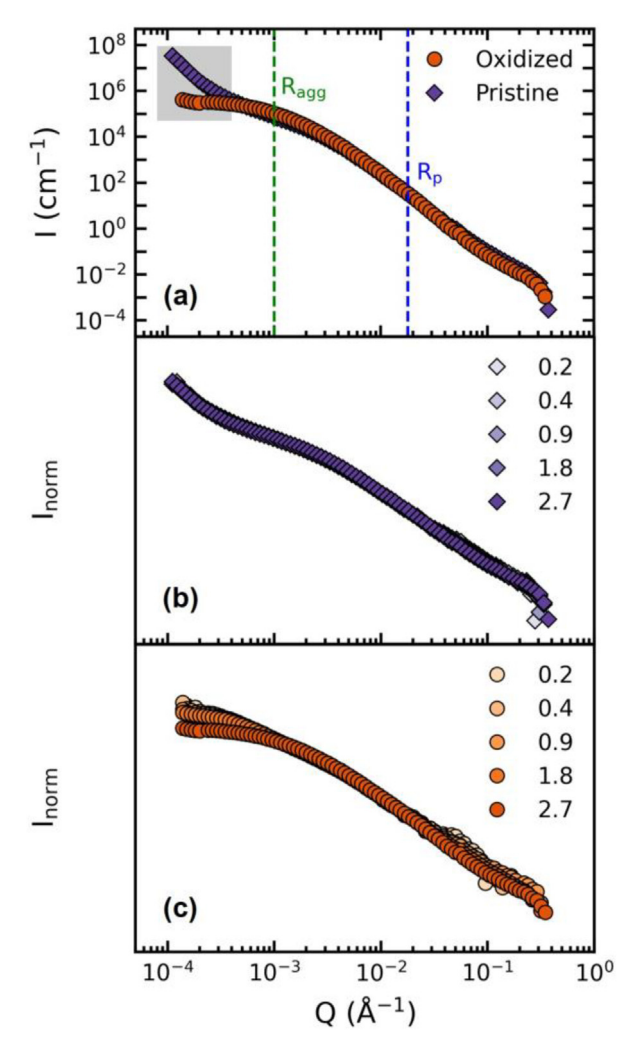


Fig. 3. (a) USAXS of pristine and oxidized CB suspensions at 2.7 wt%. The blue, dashed line denotes the average radius of the primary particles. The green, dashed line denotes the average radius of the primary aggregates. The shaded region signifies the length scale of the agglomerates. (b) Normalized scattering intensity (I_{norm}) of pristine CB suspensions at given wt%. (c) Normalized scattering intensity of oxidized CB at equivalent wt%.

by the net repulsive interaction between the immutable primary aggregates [36]. Indeed, the recovered structure factors of the oxidized suspensions, also reveal a CB content dependence (FigS5). The structure factor represents the contribution to the scattering intensity originating from the interparticle interactions acting between the primary aggregates. With increasing CB content, the structure factor falls below 1 in the limit of decreasing Q indicating the interactions are dominated by repulsive, electrostatic forces at these higher particle loadings. In contrast, the structure factors of pristine CB are all well above 1, signifying strong attraction between the primary aggregates.

3.3. Mechanical percolation

Small amplitude oscillatory shearing experiments were performed as a function of CB content for both samples to identify their respective fluid–solid transition, distinguishable by the onset of a finite elastic modulus at a critical CB content (w_c) in which mechanical percolation takes place [14]. Both the oxidized and pristine samples show this transition, with suspensions in the solid phase exhibiting a frequency independent elasticity that increases with CB content (FigS6). To identify the fluid–solid transition, the

elastic moduli at each given CB content was averaged over the measured frequency range and fit to a critical scaling law [37,38] defined as $G = \left(\frac{w - w_c}{100}\right)^q$ where q is the power law exponent. The fits are visualized in Fig. 4 with the fit parameters summarized in Table 2. The fluid-solid transition shifts from 2.8 to 7.5 wt%, possibly due to the conferred repulsive interaction that deems to maximize colloidal packing [34]. Furthermore, oxidized CB shows a much more dramatic increase in elasticity with distance from percolation. This observation can be attributed to the difference in packing behavior of the two samples. The attractive agglomerates of pristine CB have an open structure and can densify to accommodate additional CB content. On the other hand, the repulsive primary aggregates of oxidized CB resist overlapping with one another, leading to a more prominent crowding effect with increasing CB content. It is relevant to note that the power law exponents for CB in DI water are below what is reported by Trappe et al. as 4.1 in mineral oil [37] and Richards et al. as 3.2 in propylene carbonate [14], suggesting that a difference in solvent properties affects the buildup of the microstructure and the strength of the mechanical network. It is relevant to note that while oxidized CB are repulsive, a transition to a more ordered structure where packing is fully maximized is not observed due to the polydispersity of the primary aggregates.

3.4. Macroscopic behavior under flow

Having identified the CB content in which solidification occurs, rheo-electric measurements were conducted on oxidized and pristine CB suspensions that spanned the fluid-solid transition. A typical example of the results obtained from these rheo-electric tests are shown in Fig. 5 for a 7 wt% pristine CB suspension (the remaining measurements are presented in FigS7). For each shear rate of interest, a transient response in the viscosity in the form of a decay can be discerned at early times due to microstructural rearrangements (Fig. 5a). This decay in the viscosity becomes more prevalent at lower shear rates. The behavior of the transient response between high and low shear intensities is consistent with what was observed for CB dispersed in mineral oil [27] as reported by Hipp et al. This rheological behavior seen in both CB samples suspended in water suggests the presence of a nontrivial, sheardependent microstructure like those described in literature. A quasi-steady state is ultimately reached over time, and the steady state viscosity of the suspensions (η_{ss}) was thus taken as the average over the last 2 min of each shear step.

The corresponding conductivity (κ) obtained at each shear condition is the sum of the ionic contribution from the solvent (κ_{ionic}) and electronic contribution from the primary aggregates $(\kappa_{electronic})$ given as $\kappa = \kappa_{ionic} + \kappa_{electronic}$ [26]. The ionic contribution of each sample was experimentally measured, taken as the conductivity of the DI water, and subtracted from the bulk conductivity to obtain the frequency-dependent electronic conductivity of the suspension (Fig. 5b). At low frequencies, an increase in the conductivity with frequency arises due to double-layer polarization of the carbon and the electrode walls [14]. At higher frequencies, a plateau in the conductivity is observed, attributed to the migration of charges (ions and electrons) within the suspension [14]. The electronic conductivity of all suspensions was therefore taken at 40 kHz (κ_{40kHz}) where the influence of electrode polarization is minimized.

A quantitative comparison between the steady state viscosity and electronic conductivity of pristine and oxidized CB suspensions for all shear rates and CB content measured is presented in Fig. 6. In general, the viscosity of both samples increases as a function of the CB content due to the increase in contacts between primary aggregates. Pristine CB suspensions in particular exhibit a

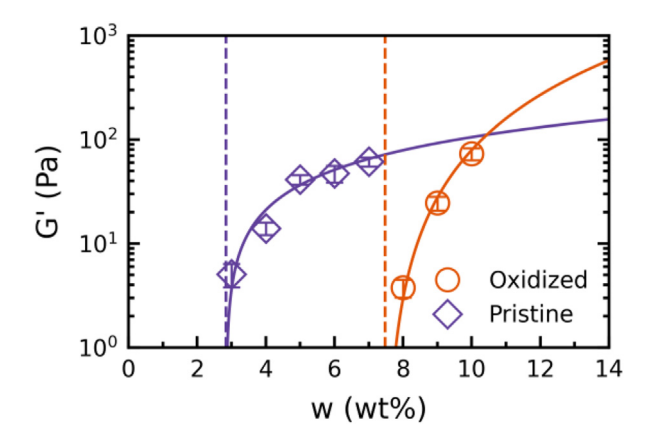


Fig. 4. The elastic modulus (G') for pristine and oxidized CB suspensions with increasing CB content (w). Error bars are 1 standard deviation from the average of 3 measurements, taken over a frequency range of 10 to 0.1 rad/s. The solid lines are fits to the percolation equation described in the text using the averages shown. The vertical, dashed lines represent the critical CB content where solidification occurs for each respective sample.

Table 2Fit parameters to the critical scaling law for pristine and oxidized CB.

Sample	q	(wt%)
Pristine XC72R	0.89	2.8
Oxidized XC72R	2.10	7.5

decrease in the viscosity as the shear rate increases across all weight fractions (Fig. 6a). This shear thinning effect, the extent of which increases for samples above w_c , is associated with the break-up of agglomerates that reduces the effective CB volume fraction in the suspension [13]. Oxidized CB suspensions also exhibit a strong shear thinning behavior above w_c due to the presence of a suspension yield stress (Fig. 6b) [39]. An apparent shear thickening regime is observed at high shear rates. We attribute this to subtle particle migration that unavoidably occurs in Couette flow [27,40]. To quantify the effects of particle migration, we compared the steady state viscosity to the viscosity of the rejuvenation step (2500 s⁻¹ preshear step). FigS8 shows that the effects of particle migration are only prevalent at the highest shear rates in the 8-10 wt% oxidized CB suspensions while remaining negligible for all other samples. Suspensions below w_c containing oxidized CB were almost Newtonian, with a weak shear thinning behavior also discernable for 5-7 wt%. Previous studies have shown that shortrange repulsive interactions enhance the zero-shear viscosity of electrostatically stable suspensions by inducing an effective volume fraction [41,42]. As high-shear viscosities depend primarily on long-range hydrodynamic interactions, it becomes insensitive to interparticle repulsion [43]. This leads to the shear thinning behavior observed in the oxidized CB fluid suspensions.

At all conditions, a finite electronic conductivity is observed that increases with CB content (Fig. 6c and 6d), consistent with prior studies for CB suspended in light mineral oil [44], ethylene carbonate [45], and propylene carbonate [46]. Electrical percolation is achieved even in the fluid phases where electron hopping between CB particles facilitates charge transport [47,48]. This framework is reliant on tunneling paths that connect when a critical separation distance is achieved between particles, which has been proven to describe the macroscopic conductivity of carbonaceous conductive additives in a filled-polymer matrix [49]. What is surprising to observe is that the electrical properties of both samples are relatively independent of the shear rate regardless of the suspension phase. These results suggest that the electrical transport of CB in neat DI water is insensitive to the primary aggregate microstructure that forms and restructures with shear flow. While CB suspensions in mineral oil were reported to show a strong dependence of the conductivity with shear rate [44–46], aqueous suspensions of CB were previously shown to have no flow rate dependence in a pressure driven flow cell [50], further implying that the suspending medium pays a non-trivial role in the electronic conductivity.

3.5. Performance as a conductive additive

To compare the effect of oxidation on the rheo-electric behavior of oxidized and pristine CB suspensions, the conductivity and viscosity values at each shear rate and CB content was parametrically plotted in Fig. 7a. Representing the data in this way defines the accessible property space for both carbon samples and allows for direct comparison. As discussed in the previous section, an increase in CB content leads to a rise in both the viscosity and conductivity of the suspensions. This results in an unfavorable trajectory in the plot to the top left region whereas the desired performance exists in the lower right region. For fluid suspensions containing oxidized CB, we observed a reduced viscosity and enhanced conductivity as compared to the equivalent pristine sample. This finding suggests that electrostatic stability enhances charge transport while preventing agglomeration and reducing viscosity. However, once mechanical percolation is achieved for both samples, this trend is not maintained. The divergence of the viscosity is steeper for oxidized CB indicating a more rapid transition to maximum packing. We believe that this is a result of the repulsive

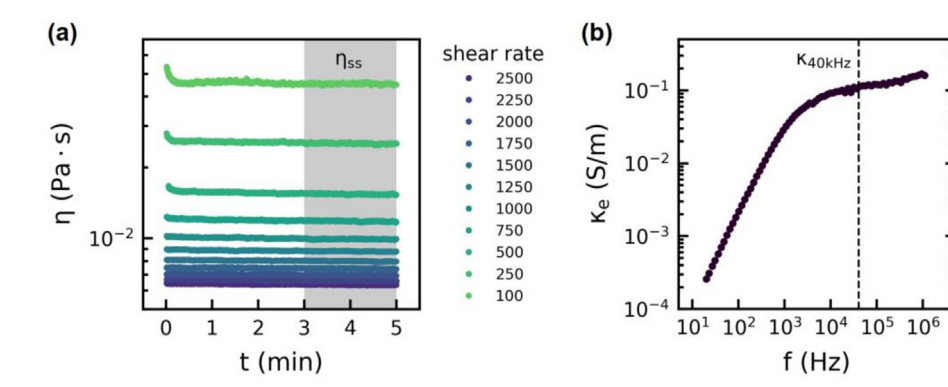


Fig. 5. (a) Evolution of the viscosity (η) over time for a 7 wt% pristine CB suspension at several shear intensities. The shaded region signifies the steady state regime of the response (η_{ss}). (b) Frequency sweep (f) of the electronic conductivity (κ_e) of the same suspension sheared at 2500 s. The vertical, dashed line denotes the electronic conductivity at 40 kHz (κ_{40kHz}).

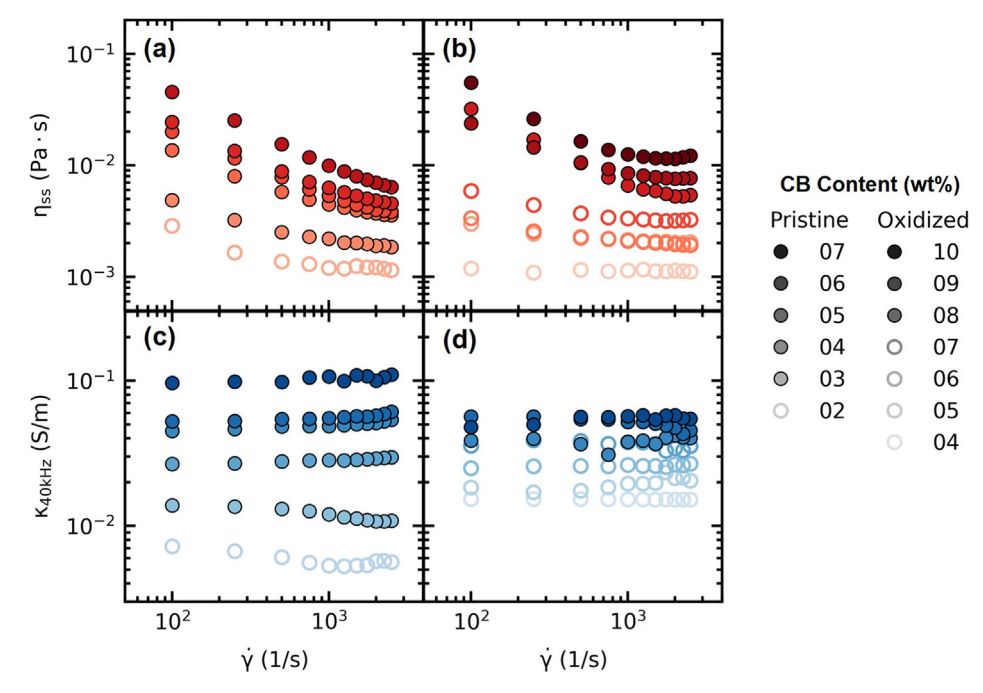


Fig. 6. Viscosities $(\eta_{ss})[(a))$ pristine, (b) oxidized] along with the associated electronic conductivities $(\kappa_{40kHz})[(c))$ pristine, (d) oxidized] of CB suspensions at given CB content as a function of shear intensity. For all plots, open and closed symbols denote a suspension in the fluid or solid phase respectively.

forces between the primary aggregates that produces a compact, glassy state that increases the barrier to structural rearrangement under flow. In fact, the maximum achievable conductivity of the pristine CB exceeds that of the oxidized samples at the same CB loading when sheared at 2500 s^{-1} (Fig. 7b). What is more striking is that the increase in the conductivity as a function of the CB content is drastically lower even when mechanical percolation is achieved. At this high-level shear intensity, the agglomerates within suspension should be significantly reduced in size. The number density of unbound primary aggregates between the two samples should therefore be similar, and the disparity in the conductivity can be explained by the difference in the interaction potentials. Under these two assumptions, we believe that the difference in conductivity results from the frequency of the primary aggregates to come into distance with one another to allow for electron hopping to occur. This hopping distance, often referred to as the characteristic tunneling distance, is in the order of 1 nm for CB [49]. Due to electrostatic forces, repulsive primary aggregates are less often able to come within hopping distance resulting in a reduced probability of transport between each other as the interaction potential is substantially large at this length scale. We believe that disassociation of the fractal agglomerates disconnects established tunneling paths in the suspension. Electrical migration from one primary aggregate to another thus occurs less frequently for oxidized CB, leading to the decrease in the rise of the electronic conductivity with particle loading.

4. Conclusions

In summary, we oxidized Vulcan XC72R carbon black resulting in the deposition of oxygen functional groups, most notably carboxyl groups, on the surface. The resulting increase in the surface charge density led to electrostatic stability and a repulsive interaction between the primary aggregate building blocks. Ultra-small-angle X-ray scattering of the carbon black microstructure quantitively confirmed inhibition of the development of the micronscale agglomerates often hypothesized in previous work of func-

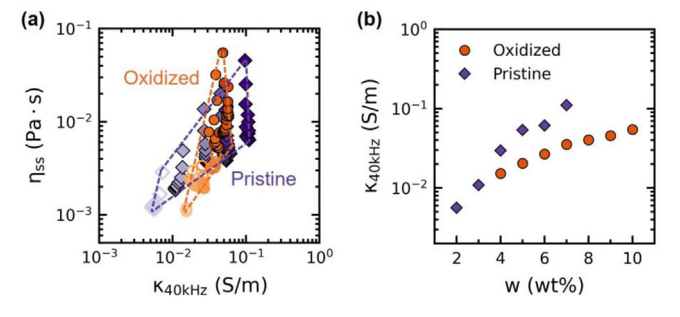


Fig. 7. (a) Viscosity (η_{ss}) and conductivity (κ_{40kHz}) pairings for pristine and oxidized CB suspensions sheared between 100 and 2500 s⁻¹. Open and closed symbols denote a suspension in the fluid or solid phase respectively. Increasing symbol contrast indicates a rising CB content. The dashed lines represent the boundaries of our measurements and are meant to guide the eyes. (b) Electronic conductivities of CB suspensions sheared at 2500 s⁻¹ as a function of CB content (w).

tionalized nanocarbon materials [17,19,20]. Electrostatic stability also led to a shift in the onset of solidification for carbon black suspensions from 2.8 to 7.5 wt%, granting access to higher carbon black content previously unattainable for aqueous suspensions [50,51]. We further probed the rheo-electric behavior of pristine and oxidized Vulcan XC72R suspended in deionized water that span their respective mechanical percolation regime. We analyzed the parametrically paired electronic conductivities and steady state viscosities at each shear rate and formulated low-viscosity, high-conductivity fluid suspensions. Unfortunately, at higher carbon black content relative to flow-electrode capacitive deionization applications, the rise in the viscosity for oxidized carbon black is higher relative to pristine carbon black due to the improved maximum packing of the primary aggregates.

The observed rheo-electric behavior of oxidized carbon black suspended in water implies that while electrical percolation is maintained with the stable primary aggregates, conduction through the attractive agglomerates is more favorable. In accordance with the critical path method [49], we believe that the frequency of electron tunneling, the mechanism for charge

transport, is lessened due to the increase in the average separation distance between primary aggregates. This agrees with the notion that agglomerate breakdown results in a decrease in conductivity [44,51]; here in our oxidized system presents the case of a fully broken-down agglomerate structure. However, the independence of the conductivity on the shear intensity and conflicting unresolved trends in literature [45,46] leads us to believe that the microstructure is only one of the underlying causes that influences charge transport. Further study into how the material properties of the carbon black conductive additive and the suspending medium is necessary in predicting the rheo-electric performance of flow electrodes. Nevertheless, our findings link the so far under studied interaction between the primary aggregates to the suspension macroscopic properties and give insight towards design rules for low-viscosity, high-conductivity flow electrodes.

CRediT authorship contribution statement

Paolo Zapanta Ramos: Methodology, Investigation, Validation, Visualization, Writing – original draft. **Connor Clayton Call:** Methodology, Investigation. **Lauren Virginia Simitz:** Methodology, Investigation. **Jeffrey John Richards:** Supervision, Conceptualization, Writing – review & editing.

Data availability

Data will be made available on request.

Declaration of Competing Interest

The authors declare the following financial interests/personal relationships which may be considered as potential competing interests: Jeffrey John Richards reports financial support was provided by National Science Foundation. Jeffrey John Richards reports equipment, drugs, or supplies was provided by Argonne National Laboratory Advanced Photon Source.

Acknowledgements

This material is based upon work supported by the National Science Foundation under Grant No. (CBET-2047365) and (DMR-1720139-006). This work made use of the NUFAB facility of Northwestern University's NUANCE Center, which has received support from the SHyNE Resource (NSF ECCS-2025633), the IIN, and Northwestern's MRSEC program (NSF DMR-1720139). This research used resources of the Advanced Photon Source (APS), a U.S. Department of Energy (DOE) Office of Science user facility operated for the DOE Office of Science by Argonne National Laboratory under Contract No. (DE-AC02-06CH11357). We would like to additionally thank Jan Ilavsky for his assistance in running remote experiments at APS.

Appendix A. Supplementary data

Supplementary data to this article can be found online at https://doi.org/10.1016/j.jcis.2022.12.017.

References

- A. Rommerskirchen, C.J. Linnartz, F. Egidi, S. Kendir, M. Wessling, Flowelectrode capacitive deionization enables continuous and energy-efficient brine concentration, Desalination. 490 (2020), https://doi.org/10.1016/j. desal.2020.114453 114453.
- [2] K.B. Hatzell, M. Boota, Y. Gogotsi, Materials for suspension (semi-solid) electrodes for energy and water technologies, Chem. Soc. Rev. 44 (2015) 8664–8687, https://doi.org/10.1039/c5cs00279f.

- [3] C. Zhang, J. Ma, L. Wu, J. Sun, L. Wang, T. Li, T.D. Waite, Flow Electrode Capacitive Deionization (FCDI): Recent Developments, Environmental Applications, and Future Perspectives, Environ. Sci. Technol. 55 (2021) 4243– 4267, https://doi.org/10.1021/acs.est.0c06552.
- [4] H. Shi, Activated carbons and double layer capacitance, Electrochim. Acta. 41 (1996) 1633–1639, https://doi.org/10.1016/0013-4686(95)00416-5.
- [5] B. Kastening, W. Schiel, M. Henschel, Electrochemical polarization of activated carbon and graphite powder suspensions, J. Electroanal. Chem. Interfacial. Electrochem. 191 (1985) 311–328, https://doi.org/10.1016/S0022-0728(85) 80025-5
- [6] B. Akuzum, P. Singh, D.A. Eichfeld, L. Agartan, S. Uzun, Y. Gogotsi, E.C. Kumbur, Percolation Characteristics of Conductive Additives for Capacitive Flowable (Semi-Solid) Electrodes, ACS. Appl. Mater. Interfaces. 12 (2020) 5866–5875, https://doi.org/10.1021/acsami.9b19739.
- [7] V.E. Brunini, Y.M. Chiang, W.C. Carter, Modeling the hydrodynamic and electrochemical efficiency of semi-solid flow batteries, Electrochim. Acta. 69 (2012) 301–307, https://doi.org/10.1016/j.electacta.2012.03.006.
- [8] S.A. Hawks, A. Ramachandran, S. Porada, P.G. Campbell, M.E. Suss, P.M. Biesheuvel, J.G. Santiago, M. Stadermann, Performance metrics for the objective assessment of capacitive deionization systems, Water. Res. 152 (2019) 126–137, https://doi.org/10.1016/j.watres.2018.10.074.
- [9] H. Parant, G. Muller, T. le Mercier, J.M. Tarascon, P. Poulin, A. Colin, Flowing suspensions of carbon black with high electronic conductivity for flow applications: Comparison between carbons black and exhibition of specific aggregation of carbon particles, Carbon. N. Y. 119 (2017) 10–20, https://doi. org/10.1016/j.carbon.2017.04.014.
- [10] B. Marinho, M. Ghislandi, E. Tkalya, C.E. Koning, G. de With, Electrical conductivity of compacts of graphene, multi-wall carbon nanotubes, carbon black, and graphite powder, Powder. Technol. 221 (2012) 351–358, https://doi. org/10.1016/j.powtec.2012.01.024.
- [11] P.C. Ma, M.Y. Liu, H. Zhang, S.Q. Wang, R. Wang, K. Wang, Y.K. Wong, B.Z. Tang, S.H. Hong, K.W. Paik, J.K. Kim, Enhanced electrical conductivity of nanocomposites containing hybrid fillers of carbon nanotubes and carbon black, ACS. Appl. Mater. Interfaces. 1 (2009) 1090–1096, https://doi.org/10.1021/am9000503.
- [12] J. Ma, C. Zhang, F. Yang, X. Zhang, M.E. Suss, X. Huang, P. Liang, Carbon Black Flow Electrode Enhanced Electrochemical Desalination Using Single-Cycle Operation, Environ. Sci. Technol. 54 (2020) 1177–1185, https://doi.org/ 10.1021/acs.est.9b04823.
- [13] J.B. Hipp, J.J. Richards, N.J. Wagner, Direct measurements of the microstructural origin of shear-thinning in carbon black suspensions, J. Rheol. (N. Y. N. Y). 65 (2021) 145–157, https://doi.org/10.1122/8.0000089.
- [14] J.J. Richards, J.B. Hipp, J.K. Riley, N.J. Wagner, P.D. Butler, Clustering and Percolation in Suspensions of Carbon Black, Langmuir. 33 (2017) 12260– 12266, https://doi.org/10.1021/acs.langmuir.7b02538.
- [15] R.R. Dagastine, D.C. Prieve, L.R. White, Calculations of van der Waals forces in 2-dimensionally anisotropic materials and its application to carbon black, J. Colloid. Interface. Sci. 249 (2002) 78–83, https://doi.org/10.1006/ jcis.2002.8239.
- [16] Y. Han, G. Hwang, S. Park, A. Gomez-Flores, E. Jo, I.C. Eom, M. Tong, H. Kim, H. Kim, Stability of carboxyl-functionalized carbon black nanoparticles: the role of solution chemistry and humic acid, Environ. Sci. Nano. 4 (2017) 800–810, https://doi.org/10.1039/c6en00530f.
- [17] K.B. Hatzell, M.C. Hatzell, K.M. Cook, M. Boota, G.M. Housel, A. McBride, E.C. Kumbur, Y. Gogotsi, Effect of oxidation of carbon material on suspension electrodes for flow electrode capacitive deionization, Environ. Sci. Technol. 49 (2015) 3040–3047, https://doi.org/10.1021/es5055989.
- [18] M. Seredych, D. Hulicova-Jurcakova, G.Q. Lu, T.J. Bandosz, Surface functional groups of carbons and the effects of their chemical character, density and accessibility to ions on electrochemical performance, Carbon. N. Y. 46 (11) (2008) 1475–1488.
- [19] Y. Cai, X. Zhao, Y. Wang, D. Ma, S. Xu, Enhanced desalination performance utilizing sulfonated carbon nanotube in the flow-electrode capacitive deionization process, Sep. Purif. Technol. 237 (2020), https://doi.org/ 10.1016/j.seppur.2019.116381 116381.
- [20] A. Schierz, H. Zänker, Aqueous suspensions of carbon nanotubes: Surface oxidation, colloidal stability and uranium sorption, Environmental. Pollution. 157 (2009) 1088–1094, https://doi.org/10.1016/j.envpol.2008.09.045.
- [21] S.W. Lee, B.M. Gallant, Y. Lee, N. Yoshida, D.Y. Kim, Y. Yamada, S. Noda, A. Yamada, S.H. Yang, Self-standing positive electrodes of oxidized few-walled carbon nanotubes for light-weight and high-power lithium batteries, Energy, Environ. Sci. 5 (2012) 5437–5444, https://doi.org/10.1039/c1ee02409d.
- [22] K. Dullaert, J. Mewis, Stress jumps on weakly flocculated dispersions: Steady state and transient results, J. Colloid. Interface. Sci. 287 (2005) 542–551, https://doi.org/10.1016/j.jcis.2005.02.018.
- [23] J. Ilavsky, F. Zhang, A.J. Allen, L.E. Levine, P.R. Jemian, G.G. Long, Ultra-small-angle X-ray scattering instrument at the advanced photon source: History, recent development, and current status, Metall. Mater. Trans. A. Phys. Metall. Mater. Sci. 44 (1) (2013) 68–76.
- [24] J. Ilavsky, F. Zhang, R.N. Andrews, I. Kuzmenko, P.R. Jemian, L.E. Levine, A.J. Allen, Development of combined microstructure and structure characterization facility for in situ and operando studies at the advanced photon source, J. Appl. Crystallogr. 51 (3) (2018) 867–882.
- [25] J. Ilavsky, Nika: Software for two-dimensional data reduction, J. Appl. Crystallogr. 45 (2) (2012) 324–328.

- [26] J.J. Richards, N.J. Wagner, P.D. Butler, A strain-controlled RheoSANS instrument for the measurement of the microstructural, electrical, and mechanical properties of soft materials, Review. of. Scientific. Instruments. 88 (10) (2017) 105115.
- [27] J.B. Hipp, J.J. Richards, N.J. Wagner, Structure-property relationships of sheared carbon black suspensions determined by simultaneous rheological and neutron scattering measurements, J. Rheol. (N. Y. N. Y). 63 (2019) 423–436, https://doi.org/10.1122/1.5071470.
- [28] D. Pantea, H. Darmstadt, S. Kaliaguine, C. Roy, Electrical conductivity of conductive carbon blacks: Influence of surface chemistry and topology, Appl. Surf. Sci. 217 (2003) 181–193, https://doi.org/10.1016/S0169-4332(03)00550-6
- [29] S.M. Senthil Kumar, J. Soler Herrero, S. Irusta, K. Scott, The effect of pretreatment of Vulcan XC-72R carbon on morphology and electrochemical oxygen reduction kinetics of supported Pd nano-particle in acidic electrolyte, Journal. of. Electroanalytical. Chemistry. 647 (2010) 211–221, https://doi.org/ 10.1016/j.jelechem.2010.05.021.
- [30] S.R. Kelemen, K.D. Rose, P.J. Kwiatek, Carbon aromaticity based on XPS II to II* signal intensity, Appl. Surf. Sci. 64 (2) (1993) 167–174.
- [31] Y. Zhang, A. Narayanan, F. Mugele, M.A. Cohen Stuart, M.H.G. Duits, Charge inversion and colloidal stability of carbon black in battery electrolyte solutions, Colloids. Surf. A. Physicochem. Eng. Asp. 489 (2016) 461–468.
- [32] M.L. Jiménez, Á.V. Delgado, J. Lyklema, Hydrolysis versus ion correlation models in electrokinetic charge inversion: Establishing application ranges, Langmuir. 28 (17) (2012) 6786–6793.
- [33] S.W. Lee, B.S. Kim, S. Chen, Y. Shao-Horn, P.T. Hammond, Layer-by-layer assembly of all carbon nanotube ultrathin films for electrochemical applications, J. Am. Chem. Soc. 131 (2009) 671–679, https://doi.org/ 10.1021/ja807059k.
- [34] J. Mewis, N.J. Wagner, Colloidal suspension rheology, Colloidal Suspension, Rheology. 9780521515 (2011) 1–393, https://doi.org/10.1017/ CP00780511077078
- [35] R. Gloukhovski, M.E. Suss, Measurements of the Electric Conductivity of MWCNT Suspension Electrodes with Varying Potassium Bromide Electrolyte Ionic Strength, J. Electrochem. Soc. 167 (2020), https://doi.org/10.1149/1945-7111/ab6a88 020528.
- [36] J.S. Pedersen, Analysis of small-angle scattering data from colloids and polymer solutions: Modeling and least-squares fitting, Adv. Colloid. Interface. Sci. 70 (1997) 171–210.
- [37] V. Trappe, D.A. Weitz, Scaling of the viscoelasticity of weakly attractive particles, Phys. Rev. Lett. 85 (2) (2000) 449–452.
- [38] V. Trappe, V. Prasad, L. Cipelletti, P.N. Segre, D.A. Weitz, Jamming phase diagram for attractive particles, Nature. 411 (6839) (2001) 772–775.

- [39] G. Ovarlez, L. Tocquer, F. Bertrand, P. Coussot, Rheopexy and tunable yield stress of carbon black suspensions, Soft. Matter. 9 (2013) 5540–5549, https://doi.org/10.1039/c3sm27650c.
- [40] W. Wolthers, D. van den Ende, M.H.G. Duits, J. Mellema, The viscosity and sedimentation of aggregating colloidal dispersions in a Couette flow, J. Rheol. (N. Y. N. Y). 40 (1) (1996) 55–67.
- [41] F.M. Horn, W. Richtering, J. Bergenholtz, N. Willenbacher, N.J. Wagner, Hydrodynamic and colloidal interactions in concentrated charge- stabilized polymer dispersions, J. Colloid. Interface. Sci. 225 (1) (2000) 166–178.
- [42] N.J. Wagner, R. Krause, A.R. Rennie, B. D'Aguanno, J. Goodwin, The microstructure of polydisperse, charged colloidal suspensions by light and neutron scattering, J. Chem. Phys. 95 (1) (1991) 494–508.
- [43] Y.S. Lee, N.J. Wagner, Rheological properties and small-angle neutron scattering of a shear thickening, nanoparticle dispersion at high shear rates, Ind. Eng. Chem. Res. 45 (21) (2006) 7015–7024.
- [44] A. Helal, T. Divoux, G.H. McKinley, Simultaneous Rheoelectric Measurements of Strongly Conductive Complex Fluids, Phys. Rev. Appl. 6 (2016) 1–19, https://doi.org/10.1103/PhysRevApplied.6.064004.
- [45] A. Narayanan, F. Mugele, M.H.G. Duits, Mechanical History Dependence in Carbon Black Suspensions for Flow Batteries: A Rheo-Impedance Study, Langmuir. 33 (2017) 1629–1638, https://doi.org/10.1021/acs.langmuir.6b04322.
- [46] M. Youssry, L. Madec, P. Soudan, M. Cerbelaud, D. Guyomard, B. Lestriez, Non-aqueous carbon black suspensions for lithium-based redox flow batteries: Rheology and simultaneous rheo-electrical behavior, Phys. Chem. Chem. Phys. 15 (2013) 14476–14486, https://doi.org/10.1039/c3cp51371h.
- [47] C. Li, E.T. Thostenson, T.-W. Chou, Dominant role of tunneling resistance in the electrical conductivity of carbon nanotube-based composites, Appl. Phys. Lett. 91 (22) (2007) 223114.
- [48] S. Kirkpatrick, Classical Transport in Disordered Media: Scaling and Effective-Medium Theories, Phys. Rev. Lett. 27 (1971) 1722–1725, https://doi.org/10.1103/PhysRevLett.27.1722.
- [49] G. Ambrosetti, C. Grimaldi, I. Balberg, T. Maeder, A. Danani, P. Ryser, Solution of the tunneling-percolation problem in the nanocomposite regime, Phys. Rev. B. Condens. Matter. Mater. Phys. 81 (2010) 1–12, https://doi.org/10.1103/ PhysRevB.81.155434.
- [50] M.S. Alfonso, H. Parant, J. Yuan, W. Neri, E. Laurichesse, K. Kampioti, A. Colin, P. Poulin, Highly conductive colloidal carbon based suspension for flow-assisted electrochemical systems, IScience. 24 (5) (2021), https://doi.org/10.1016/j.isci.2021.102456.
- [51] M. Meslam, A.A. Elzatahry, M. Youssry, Promising aqueous dispersions of carbon black for semisolid flow battery application, Colloids Surf A Physicochem Eng Asp. 648 (2022). https://doi.org/10.1016/ j.colsurfa.2022.129376.